Reduction of Parasitic Currents in Simulation of Droplet Secondary Breakup with Density Ratio Higher than 60 by InterDyMFoam

S. Tavangar, S.H. Hashemabadi, A. Saberimoghadam*
CFD Research Laboratory, School of Chemical Engineering, Iran University of Science
And Technology, Tehran, Iran

Abstract

Secondary breakup of Newtonian droplet into continuous air jet was numerically studied. A coupled Large Eddy Simulation (LES)/ Volume of Fluid (VOF) technique was used in this investigation. Dynamic adaptive mesh was also employed. To this end, the open source CFD package, OpenFOAM, was used to perform the numerical study and was modified to meet the needs of the problem. In order to reduce the error, resulting from the spurious currents, Laplacian smoothing filter was used, which transforms the volume fraction into a smoother volume fraction. This filtering process also helped to obtain a sharp fluid interface. The smoothing has qualitatively and quantitatively improved the simulation results in bag breakup regime. Comparing the results of the RNG k-ε turbulence model and LES model showed the great influence of LES model to improve results. The detailed physics of two different breakup regimes, i.e. bag and multimode (streamer) were investigated. The numerical drop breakup regimes showed appropriate agreement with experimental observation. According to the analogy between the secondary and primary atomization, the outcomes can be used for development of the atomization models.

Keywords: *Secondary Breakup of Newtonian Droplet, VOF/LES, Bag and Multimode Regimes, OpenFoam*

1. Introduction

Atomization involves the conversion of fluid jet into a dispersion of fine droplets to form a spray. It comprises primary and secondary atomization stages [1]. Primary atomization, leads in the first few diameters from the nozzle exit, where the liquid jet displays large-scale coherent structure interaction with gas phase [2]. In secondary atomization, aerodynamic forces and surface turbulence break down the ligaments to even smaller droplets. Since atomization mainly aims to achieve the desired droplet size distribution, it is critical to identify conditions and factors affecting droplet size. On the other hand, atomization has applications in a wide variety of industrial fields such as the combustion process [2], coating, agriculture, polymer industry [1], and liquid-liquid extraction [2]. Therefore, determination of factors influencing droplet size and disintegration of ligaments into droplets will play a vital role in increasing industrial efficiency and reducing costs. Moreover, in presence of a high velocity fluid adjacent to

---

∗Corresponding author: hashemabadi@iust.ac.ir

the jet, droplet and jet breakups are very similar [3-4]. The breakup regimes of a round liquid jet in gaseous crossflow have a good analogy with those of a single drop in uniform gaseous flow [5]. Secondary breakup can be evaluated through three experimental methods including collision of a high velocity continuous jet with fluid ligament, using the shock wave generated by bursting the diaphragm of a shock tube, and vertical movement of the droplet by the gravitational force[1]. Owing to the results of such experiments, shape change and secondary breakup of the droplets can now be described in terms of two dimensionless parameters called Weber number (We_d) and Ohnesorge number (Oh) [2]. We_d is defined as the ratio of inertial forces to surface tension forces:

$$We_d = \frac{\rho_g u_g^2 D_0}{\sigma} \qquad (1)$$

Where, ρ_g, D_0, u_g, and σ are gas phase density, initial droplet diameter, gas velocity, and surface tension, respectively. Oh is expressed as the ratio of viscous forces to surface tension and inertial forces:

$$Oh = \frac{\mu_d}{\sqrt{\rho_d \sigma D_0}} \qquad (2)$$

Where, ρ_d and μ_d are droplet density and viscosity, respectively. Experimental regimes of the secondary breakup of droplets with Oh < 0.1 (non-viscous) are shown in Fig. 1(a) [1]. As seen, with We_d < 12, the droplet vibrates and splits after a relatively long time compared to other mechanisms. When 20 < We_d< 50, the droplet transforms from a spherical shape into one or several

overlapping bags and breaks up first from the inside and then from the basal rim. Different mechanisms such as bag stamen, sheet thinning, and shear have been suggested based on the various shapes created in this range [6-7]. Bag breakup occurs at low We_d. Therefore, minimal energy is needed to achieve secondary atomization. For this reason, bag breakup is perhaps the most important mode, and the We_d marking the start of bag breakup has been termed the critical Weber number, We_{dc}[2]. When 50 < We_d>1000, the droplet takes the shape of a saucer whose edges are in the opposite direction of the flow. Breakup will then begin from the indented edges of the saucer. At this stage, increased We_d will be associated with further indentation of the saucer toward its center. Finally, when We_d> 1000, the saucer will be divided into three parts which will each then break up into smaller droplets based on Rayleigh-Taylor instability. However, the mentioned ranges of We_d are not fixed and changes in various mechanisms may gradually occur [1]. According to Figs. 1 (b), the comparison of primary and secondary breakup regimens revealed that the bag, shear, and catastrophic breakup regimens of the secondary breakup were largely analogous to liquid jet in gaseous crossflow in terms of the range of critical Weber number. However, it should be noted that the gas velocity was replaced with the velocity of liquid jet in Weber number for jet. The analogy between the primary and the secondary breakup associated with the dimensionless Weber number, and similar phenomena in droplet and jet would occur when the proportion of inertial forces was close to the proportion

surface tension [3-5]. When Ohnesorge number is greater than 0.1, or spray liquid has non-Newtonian properties, the critical Weber numbers of the secondary breakup regimens do not obey the values shown in Fig. 1(a), and borderline Weber numbers obey the value of Ohnesorge number. Under such a condition, using the analogy between the primary and secondary breakup and the information on the secondary breakup phenomenon would be an appropriate strategy for adjusting the conditions of the process to reach finer droplets. Due to the presence of spatial and temporal constraints, the exact mechanisms of geometric deformation of moving droplets in different regimes have not been experimentally clarified [7]. Considering the existing limitations, numerical analysis techniques, e.g. the volume of fluid (VOF) [7-10] can be used to determine the causes of secondary breakup and to control the phenomenon. Meanwhile, experts have introduced direct numerical solution based on the VOF method as the best technique for simulation of droplet deformation and breakup [1, 7]. In this method, the species transport and conservation equations are solved to track the free surface between two immiscible phases and to determine value of each phase in computational cells [11]. In recent years, this method has been used to investigate the deformation and breakup of Newtonian droplets in unidirectional flows, as in the vertical motion test where the ratio between the densities of the two phases is assumed to be less than 10 [7, 9]. Despite the advantages of the VOF method, such as satisfying the conditions of conservation of mass in solving conservation of mass and momentum equation, an unphysical current called parasitic or spurious current is a major challenge to the method, especially when the ratio between the density of the two phases is high [12].In the momentum equation, the current is generated from determination of the magnitude of curvature at the interface. The application of the adaptive mesh refinement [13], subgrid-scale (in Large Eddy simulation) [14], and smoothing of volume fraction [15] methods will decrease the magnitude of this current.
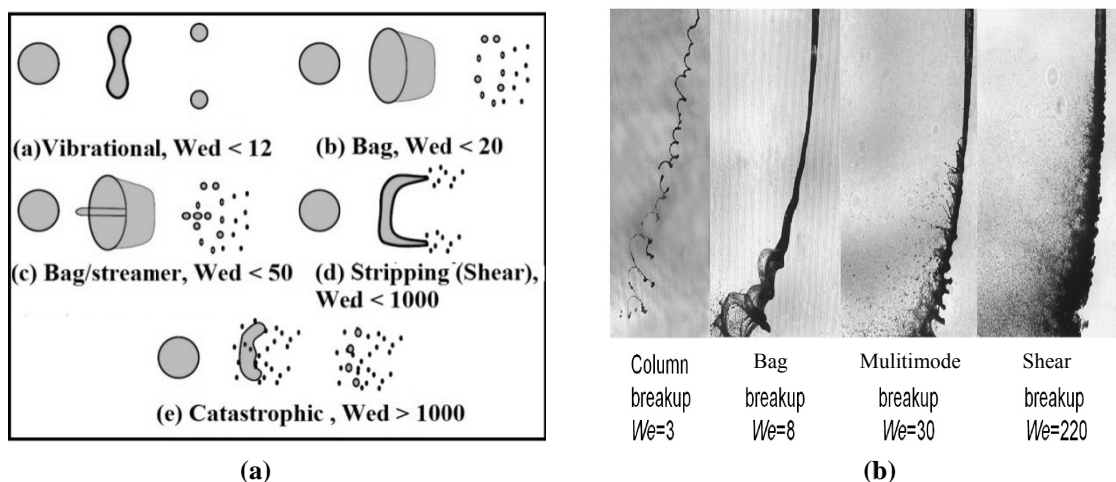

(a)

(b)

Figure 1. (a) Secondary droplet breakup regimes [2], (b) breakup regimes of one round liquid jet in gaseous crossflow [5].

To the best of our knowledge, no comprehensive analysis of droplet breakup in airstream with a density ratio of greater than 60 and under continuous jet conditions has been previously performed. A high density ratio will lead to unstable numerical solution at the interface with high deformation, and large cell dimensions [16]. Evaluating such circumstances is essential when the assumption of low density ratio cannot be satisfied. Further experimental data are needed to address the accuracy of these simulations in low density ratio [1]. The advantage of using continuous jet method in studying the secondary breakup phenomenon against other methods is also its simplicity and the possibility to accurately record the information on how a droplet moves in the continuous flow of gas. Simulation of the secondary breakup of the droplet in the shock tube experiment faces problems in analyzing the accuracy of results due to the sudden generation of the shock wave and lack of accurate information on the path and velocity of the droplet.

The present study used the Laplacian smoothing technique [15] to reduce parasitic current in the LES/VOF method with adaptive dynamic mesh. It also assessed the effects of this technique on simulation of VOF by a series of tests on the new solver. Bag and multimode regimes of secondary breakup of Newtonian droplets under continuous jet conditions and high density ratio between the two phases were then evaluated.

2. Governing equations
2-1. VOF method
The VOF method locates the interface of two immiscible, incompressible phases by

considering a set of equations, comprising the conservation of mass and momentum equations, for both phases. These equations relate to each phase through its volume fraction (α) [16]:

$$\nabla u = 0 \tag{3}$$

$$\left(\frac{\partial \rho(x,t) u}{\partial t} + \nabla \cdot (\rho(x,t) uu) \right) = -\nabla p +$$

$$\rho g + \nabla \cdot (\mu(x,t)[\nabla u + \nabla u^T]) + \tag{4}$$

$$\int_{S(t)} \sigma \kappa' n' \delta(x - x') dS$$

$$\left(\frac{\partial \alpha}{\partial t} + \nabla(u\alpha) \right) + \nabla \cdot [u_r \alpha(1 - \alpha)] = 0 \tag{5}$$

Where $u(u_x, u_y, u_z)$, p, g, μ, and ρ are the velocity vector, dynamic pressure, gravitational acceleration, dynamic viscosity, and density, respectively. Moreover, $\alpha(x,t)$ is the volume fraction of the fluid phase and can range between zero (for cells filled with gas) and one (for cells filled with fluid) at the interface. The continuum surface force (CSF) method suggested by Brackbill *et al.* [17] describes the effects of surface tension as a continuous transient volumetric force:

$$\int_{S(t)} \sigma \kappa' n' \delta(x - x') dS \approx \sigma \kappa \nabla \alpha \tag{6}$$

Where κ is interface curvature.

$$\kappa = \nabla \cdot \left(\frac{\nabla \tilde{\alpha}}{|\nabla \tilde{\alpha}|} \right) \tag{7}$$

In order to reduce the parasitic current in the VOF method and to ensure the correct calculation of interface curvature in equation (7), Lafaurie *et al.* [18] suggested volume

fraction (α) be replaced with its smoothed value ($\tilde{\alpha}$) based on the Laplacian filter [15]. In this method, the volume fraction of a limited region of the interface is smoothed.

$$\tilde{\alpha}_p = \frac{\sum\limits_{f=1}^{n} \alpha_f S_f}{\sum\limits_{f=1}^{n} S_f} \qquad (8)$$

Where p, f, α_f and S_f are cell index, surface index, linear interpolated volume fraction at the center of the cell surface, and cell surface area, respectively. In this method, the volume fraction in each cell is interpolated with the volume fraction of its neighbor cell (average value) and multiplied by the area of their intermediate cell, and the obtained value would be in the summation of the numerator of the Equation (8).

Since we evaluated a diffuse interface which is a 2-3-cell-thick region, instead of a line, the relative velocity of gas and liquid phases (u_r) was added to equation (5) to reduce the thickness of the interface and thus enhance its clarity [16]. The compressed term of the interface in equation (5) is only activated in the interface region. Now, u_r can be calculated as:

$$u_r = \min\left[C_\alpha |u|, \max(|u|)\right] \frac{\nabla \alpha}{|\nabla \alpha|} \qquad (9)$$

Where C_α is the interface compression constant ranging from zero to four [16]. In the current study, C_α was assumed to be 1 [15]. In the VOF method, physical properties, e.g. viscosity and density (ψ), in each computational cell depend on α in that position [17]:

$$\psi = \alpha \psi_l + (1-\alpha)\psi_g \qquad (10)$$

Where g and l represent gas and liquid phases, respectively. The above-mentioned equations were solved with the finite-volume-based open source code OpenFOAM on co-located grids [11].

2-2. Initial boundary conditions, solution and analysis of data

In order to analyze droplet breakup, the computational area was defined as in Fig. 2 (a). As seen, the droplet with the initial diameter, D_0, and initial vertical velocity, V_0, collides with and enters the air jet flowing at velocity u_g in x+ direction. The above region of the air jet has been assumed to account for initial deformation of droplet due to collision with air jet and passing through the mixing layer. Atmospheric pressure was assumed to be present in all walls of Fig. 2 (a), except x=0. Since the computational area was much larger than the droplet, a new smoothed dynamic solver referred to as smooth InterDyMFoam was used after modification to improve the smoothness of the gas–liquid interface. In the applied method, cells were smaller where high flow gradient was present (such as at the interface). The reduction in cell size at the interface was considered as two. Fig. 2 (b) depicts cell breakup at the interface on a two-dimensional plate ($z=3.5D_0$). In order to take grid motion and deformation, finite volume discretization was performed according to the arbitrary Lagrangian-Eulerian (ALE) method [13]. For effectively capturing the transient flow field and to extract a highly complex multiphase, LES (Large Eddy Simulation) strategy is exercised [19], additionally it has effects on

elimination of parasitic flow [14]. It should also be mentioned that in OpenFOAM, the high density ratio problem has been eliminated by interpolating the predicted velocity field to the cell faces [16]. The VOF–LES equations are derived from Equation (4) by filtering the momentum equations to separate the velocity field containing the large-scale components, which is achieved by filtering the velocity field. Using the one dimensional notation, the filtering velocity is defined as

$$\overline{u}(x) = \int G(x, x_1)u(x_1)dx_1 \tag{11}$$

where $G(x, x_1)$ is the localized function of the filter kernel. The eddy sizes are identified by using a length scale, Δ, in which eddies larger than Δ are roughly considered as large eddies and are resolved. The filtering of the convection term in the momentum equation creates difficulties in LES modeling because of its non-linearity. Known as subgrid scale (SGS) stress, this type represents the effects of the unresolved small scales of turbulence and is given by

$$\tau^{sgs} = \overline{uu} - \overline{u}\,\overline{u} \tag{12}$$

SGS stress must be modeled. In the present work, the one-equation eddy viscosity model (oneEqEddy) with the cubic root of volume set as filter width was used owing to its reasonable results [19]. As the results are sensitive to time steps when Courant numbers are greater than 0.2, we considered Courant number equal to 0.15 in all calculations [16]. After the calculations, important parameters for quantitative evaluation of the results including center of mass trajectory (X_{CM}) [20], Sauter mean diameter (SMD) [21] were described through equations 13-14, respectively.

$$X_{CM} = \frac{\sum_{1}^{n-cell} \alpha vol_{cell} x_{cell}}{\sum_{1}^{n-cell} vol_{cell} \alpha} \tag{13}$$

$$SMD = 6\frac{\sum_{1}^{n-cell} \alpha vol_{cell}}{\sum_{1}^{n-cell} |\nabla \alpha| vol_{cell}} \tag{14}$$

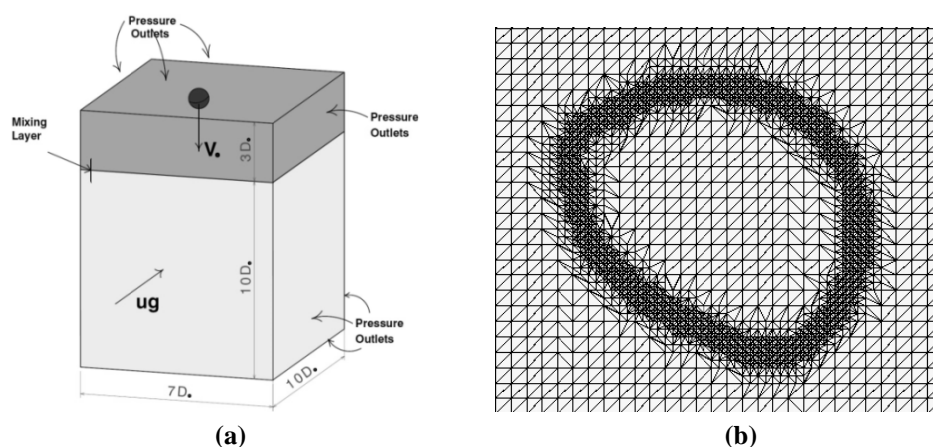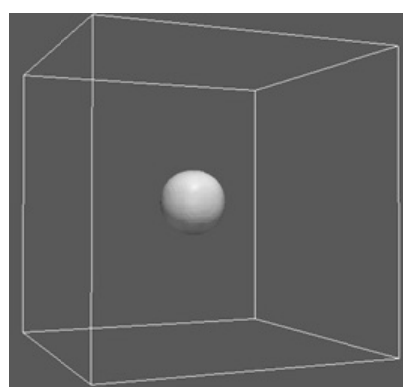Where x_{cell} and vol_{cell} are the center and volume of the cell, respectively.

Figure 2. (a) Computational domain and boundary conditions (b) a frame showing the adaptive local refined grid in $z = 5D_0$ plane.
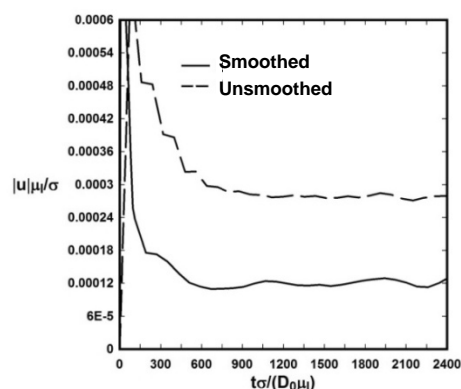
3. Numerical results

3-1. A static droplet in a quiescent fluid

The example of static droplet in a quiescent fluid without the force of gravity (g=0) was used to determine the quantitative effect of smoothing volume fraction on spurious current based on Fig. 3. The example is used to examine the accuracy of different analysis methods of two-phase flow [15, 18]. In such conditions, the droplet should not physically move in any way over time. Due to the difficulties with determining the curvature of interface and calculating the gradient of the volume fraction, Equation (4) is not converted to Young-Laplace equation, and the spurious current appears as the amount of velocity in the momentum equation. To simulate the example, dimensions of the computation domain was specified according to Fig. 3 (a) $5D_0 \times 5D_0 \times 5D_0$, and the droplet was placed in the center of the cube. The results of changing dimensionless velocity that is similar to the dimensionless capillary number of the parasitic current are shown based on the dimensionless time in Fig. 3 (b). As it is observed, smoothing with Laplacian filter reduced parasitic current by one-third.

3-2. A 2D droplet in a vortical flow field

As a second test of the smoothing algorithm, the stretching and thinning of a 2D object in a vortical flow field was simulated. This test is aimed at evaluating the capability of the solver in handling severe deformations without causing erroneous numerical breakup [16].

Initially a circle with a diameter of 0.15 is placed at (0.5, 0.75) in a 1×1 square domain, the test was performed with level of velocity

$$u_x = \sin^2(\pi.x)\sin(2\pi.y)\cos(\pi.t/T)$$
$$u_y = -\sin^2(\pi.y)\sin(2\pi.x)\cos(\pi.t/T)$$
(15)

This velocity field deforms the droplet into a thin spiraling ligament, which reaches its maximum deformation at t = T/2. As seen in Fig. 4, the smoothed simulation result depicted more continuous deformation and was closer to the phase field method results [22] compared with the unsmoothed simulation results.
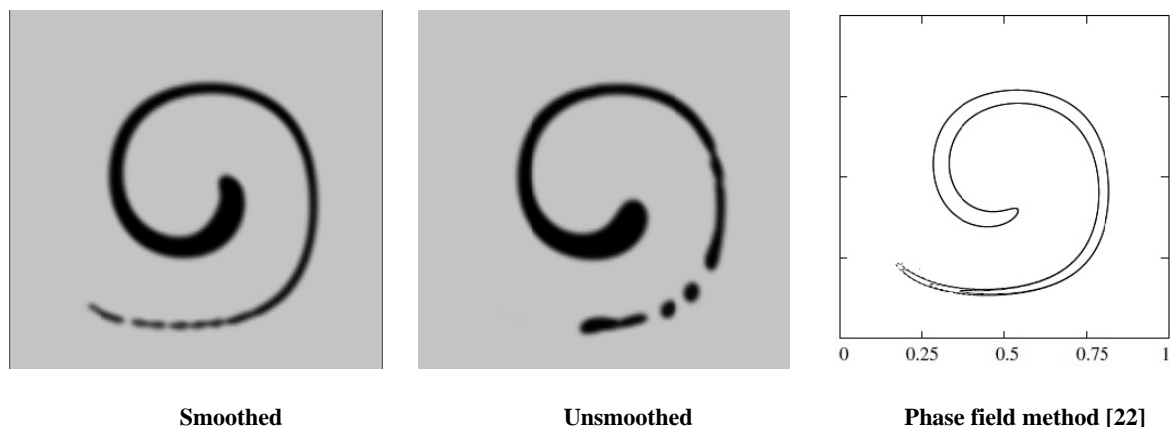

| (a) | (b) |

Figure 3. (a) Computational domain of a static droplet in a quiescent fluid, (b) Corresponding time traces of the dimensionless magnitude of parasitic currents.

| **Smoothed** | **Unsmoothed** | **Phase field method [22]** |

Figure 4. Circle undergoing deformation in a vortex at t = T/6.

3-3. Grid independency and validation

Ethanol drops in air were evaluated to identify different regimes of secondary droplet breakup [23]. Droplets of 2.33 mm in diameter with physical properties presented in Table 1 collide with a continuous air jet. In order to assess the independence of the solution from the computational grid, $D_0/10$, $D_0/14$, and $D_0/20$ sizes were considered for $We_d = 13$ and the computational area in Fig. 1 (a). The temporal growth of drop cross-stream dimension ratio (d_{cro}/D_0) [10] was determined according to Fig. 5. The numerical simulation shows, with a coarse grid ($D_0/10$) resulted in an unreliable d_{cro}/D_0 ratio. In cases $D_0/14$, and $D_0/20$, due to effects of the droplet penetration in the mixing layer, the vertical deformation of droplets at the first stage (t < 0.004s) were grid-dependent, and the scales of the d_{cro}/D_0 ratio were on the same order for the two cases. Therefore, the numerical simulation used case $D_0/14$ to reduce the calculation time. The results obtained from simulations with $We_d = 13$ and $We_d = 22$ were compared with the findings of droplet breakup experiments [23, 10] in which droplet

morphology and location at different times were assessed using shadowgraphy and particle image velocimetry [23].

Table 1. Ethanol physical properties [23] and summary of other parameters for simulations.

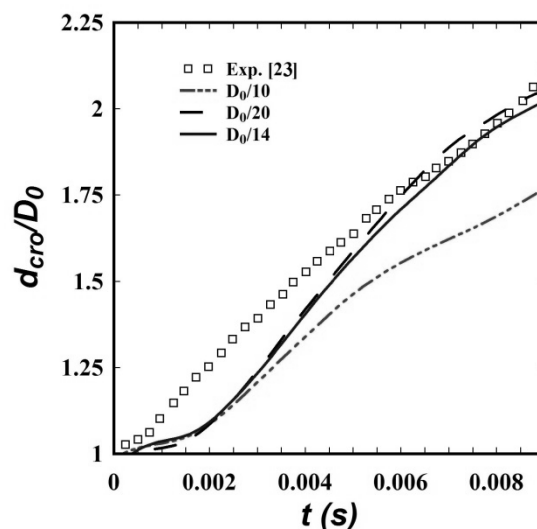| ρ_l(Kg/m³)	σ (mN/m)	μ_l (Pa.s)	We_d	Oh	Re
789	0.0223	0.0012	13	0.006	1500
			22	0.006	1950

Figure 5. Temporal growth of drop cross-stream (d_{cro}/D_0) dimension predicted on the three grids.

The results of comparisons are depicted in Figs. 6-7. As it is shown, when $We_d = 13$, a

bag breakup regime was presented and smoothing led to the formation of more stable and symmetrical bags. Moreover, the initial droplet deformation stage (the first 4 ms) and the deformation of the droplet into a saucer were highly similar to the recorded experimental images, morphologically (Figs. 6 (a), 7(a)). In other words, from the moment of bag formation until bag breakup in simulations, the smoothed simulated and experimented results were consistent (0.008 s < t < 0.0098 s, Fig. 7(b)).

In the development of the bag, the simulated results differed from the real experiment. In simulations, the parasitic flow intrinsic to the VOF method caused non-physical bag breakup, reduced pressure on the front of the
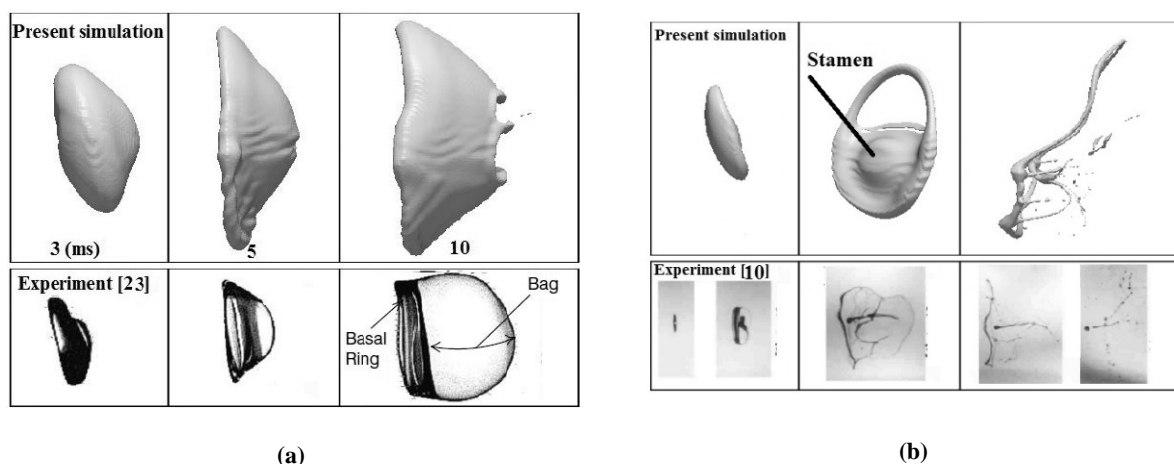

(a)

(b)

Figure 6. Comparison of numerical and experimental results [23, 10] for ethanol droplets (a) 3D illustration of predicted bag (We = 13) and (b) sheet-thinning (We = 22) breakup, air flow direction = left to right.
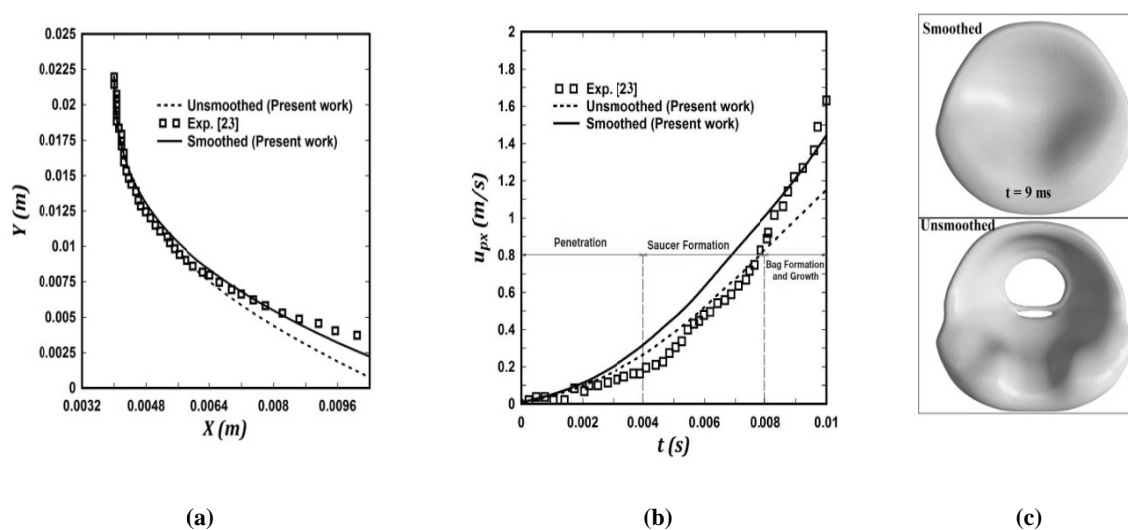

(a)

(b)

(c)

Figure 7. Comparison between the experimental[23] and numerical results, (a) Mean trajectory, (b) Horizontal velocity for bag breakup, (c) smoothing effects on morphology, Wed = 13.

droplet, and thus decreased the horizontal distance travelled by the droplet (Fig. 7 (a)). As seen in Fig. 7 (c), although breakup was delayed by smoothing, the remaining parasitic flow resulted in non-physical breakup, reduced the horizontal distance moved by the droplet, and finally lowered droplet velocity (Fig. 7 (b)). However, the smoothness did not have the improving effects on drop horizontal velocity at deformation stage and before bag formation (t < 0.008 s). On the other hand, the dimensions of the computational grid were also responsible for the differences between simulated and experimented results. In fact, holographic test results suggested the thickness of the droplet bag in the air was equal to the droplet's initial diameter multiplied by 0.04 [24]. Therefore, accurate simulation of this phenomenon required the number of initial dynamic computational cells for the initial diameter to be at least 100. Nevertheless, solving such a computational grid is rather difficult due to the existing hardware limitations. In addition, in the VOF method, severe reduction in the dimensions of computational cells is associated with a substantial increment in the parasitic flow [12]. Meanwhile, smoothing delayed bag breakup by 0.8 millisecond and also increased its depth. Consequently, the pressure on the front of the bag was maintained for a longer time and maximum horizontal velocity error decreased by 20%. Moreover, the center of mass of the droplet was determined based on the results of experimental shadowgraphy [23] in which two-dimensional images are recorded. Experimental studies [24-25] have calculated the volumetric ratio of basal ring (Fig. 6(b),

10 ms) to the droplet as 84%-92%. Such conditions have led to a minimum average error of -20% in experimental studies of droplet location from the beginning of bag formation (Fig. 7(a)). Incorporating this error in comparisons between experimental and simulation results would draw the simulated and experimental results in Figs. 7 (a, b) closer. Similar results were obtained in case of $We_d = 22$ (Fig. 6(b)). According to the droplet breakup pattern in Fig. 1(a), droplet breakup in this region followed a streamer (multimode) regime. In this regime, the stamen completely hinders part of the bag from developing and forms a multi-bag with a central stamen structure. The thickness of each bag was similar to that in the bag breakup regime. Likewise, the presence of large cells (compared to bag thickness) and errors in interface detection reduced the accuracy of simulation in predicting droplet shape.

Following the deformation of the droplet, the volume to surface ratio and SMD change. Experimental relationships for determining SMD in bag breakup regime depend on Weber number [26].

$$We_{SMD} = 0.7377 We_d^{2/3} \qquad (16)$$

Table 2. The error of the final SMD/D_0 ratio.

Case	Error
$We_d=13_{(smoothed)}$	0.06
$We_d=13_{(unsmoothed)}$	0.31
$We_d= 22_{(smoothed)}$	0.04

Where, We_{SMD} is We_d with SMD value instead of the initial droplet diameter. Hence, the final ratio of SMD to the initial diameter would be 0.317 for We_d= 13. The results of the error of the final ratio of SMD/D_0 are shown in Table 2. As seen, SMD at the final breakup time according to Equation(14), was 0.333 times initial diameter in the smoothed case and 0.426 times initial diameter in the unsmoothed case for We_d = 13. Obviously, smoothing improved final SMD value compared to its experimental value.

3-4. Turbulent model effects

The analysis of turbulent flows to determine mean velocity and value of fluctuations is generally performed on two perspectives of temporal averaging and spatial filtering of Navier-Stokes equations [2]. Unlike the temporal averaging (within a specific time), averaging is carried out for a specific spatial range in the filtering process shown in Equation (11). The priority of the first method in solving simple flows with limited deformation is its higher computational speed. Whereas in instantaneous flows where fast and instantaneous temporal changes occur in the direction of the flows and in two-phase conditions accompanied with breakup, the use of the second method is more appropriate due to its higher impact on the quality of results [14]. In this section, results of simulation using time-averaged turbulence model RNG k-ε [27] were compared to the results of the simulation performed for the droplet breakup in the Weber number 13 using the one-equation turbulence model for large eddy simulations (Fig. 8). According to the results, the turbulence model had little impact on

computing the center-of-mass position of the droplet (Fig. 8a), while the temporal functionality of the droplet's velocity droplet and morphology largely obeyed the type of turbulence model. Based on the results of RNG k-ε method, the droplet breakup regime was in the vibration regime, while regarding [23], the breakup regime in such a Weber number conformed to the bag breakup regime. Results of computing with LES turbulence model predicted the regime. Results obtained from RNG k-ε turbulence model showed the weakness of the model in determining the type of breakup regime and velocity of droplet center-of-mass. The use of subgrid filter in the model for large eddy simulations resulted in reduction of parasitic current and computation of the vortexial flow behind the droplet. Moreover, mean instantaneous velocity can be determined in the model for large eddy simulations [19]. Although the use of time-averaged turbulence model reduced the time of computations by 27% (152 h), the turbulence model for large eddy simulations should be used regarding the higher quality of its results.

4. Conclusions

In this article, secondary breakup of Newtonian ethanol droplet was studied in continuous air flow. In this simulation with high density ratio (641), Volume of Fluid method was used in combination with one-equation large eddy simulation model in a dynamic solution grid. The intrinsic spurious flow in volume of fluid method was reduced using Laplacian volume fraction averaging. From the results in the test cases it can be seen that smoothing method reduced the

error of interface-capturing. In bag and multimode breakup regimes, the results agreed with experimental results until formation of initial deformation and bag formation stage. In bag growth stage, due to residual spurious flow in solution method and inadequate break down of grid for hardware reasons, early breakup of bag was observed. This non-physical breakup led to greater difference between simulation and experimental results. Moreover, the RNG k-ε approach was also applied to model turbulence. It is shown that the accuracy of the LES results was considerably more than the RNG k-ε results. The results of predication of the final fragment SMD for drop breakup in bag and multimode regimes showed good agreement with experimental observation. According to the similarity and analogy between the secondary and primary atomization, the obtained results can be used in a wide range of engineering applications, from coating to combustion.
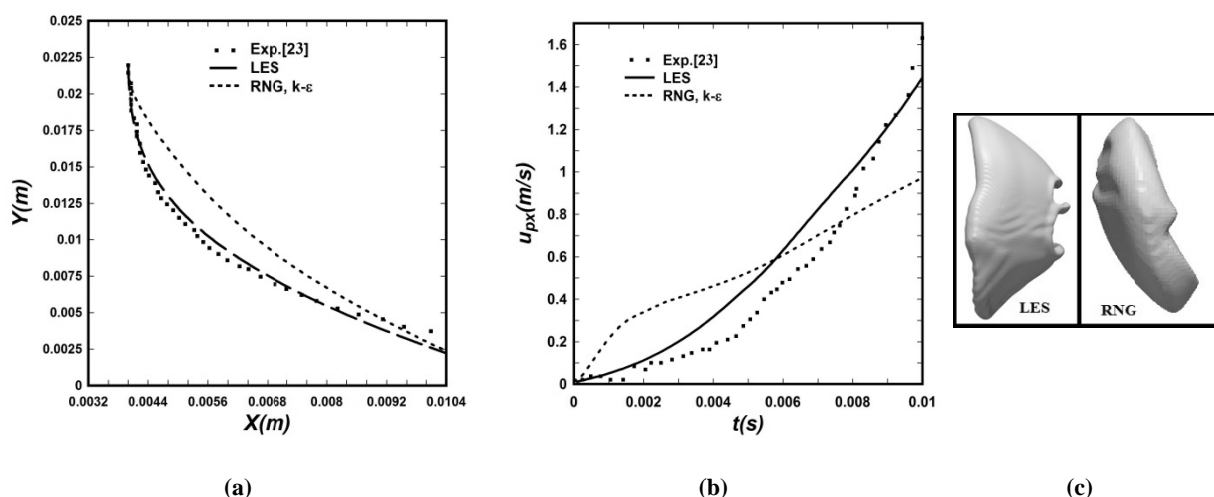

Figure 8. Comparison of LES and RNG k-ε simulation with experimental results [23]. (a) Mean trajectory, (b) Horizontal velocity, (c) droplet morphology at 10 ms, $We_d = 13$.

Nomenclature

D	Droplet diameter (m)
Oh	Ohnesorge number
P	Pressure (N/m^2)
Re	Reynolds number
S	Cell area (m^2)
SMD	Sauter mean diameter (m)
t	Time (s)
u	Velocity (m/s)
V	Vertical falling velocity (m/s)
We	Weber number
X	Center of mass (m)

Greek symbols

α	Volume fraction
κ	Curvature (1/m)
μ	Viscosity (Ns/m^2)
Δ	Filter width (m)
ρ	Density (Kg/m^3)
τ	Stress (Pa)
σ	Surface tension (N/m)

Subscript

d	Dispersed phase
f	Face
g	Gas

l   Liquid
0   Initial

Superscript

SGS   Sub grid scale

References

[1] Guildenbecher, D., Lopez-Rivera, C. and Sojka, P., "Secondary atomization", Exp. Fluids, 46(3), 371, (2009).

[2] Ashgriz, N., Handbook of atomization and sprays: Theory and applications, Springer Verlag., (2011).

[3] Farago, Z. and Chigier, N., "Morphological classification of disintegration of round liquid jets in a coaxial air stream", Atomization Sprays, 2, 137, (1992).

[4] Wang, Y., Im, K. and Fezzaa, A., "Similarity between the primary and secondary air-assisted liquid jet breakup mechanisms", Phys. Rev. Lett., 100, 154502-1, (2008).

[5] Sallam, K.A., Aalburg, C. and Faeth, G.M., "Breakup of round nonturbulent liquid jets in gaseous crossflow", AIAA J., 42, 2529, (2004).

[6] Zhao, H., Liu, H., Xu, J., Li, W. and Lin, K., "Temporal properties of secondary drop breakup in the bag-stamen breakup regime", Phys. Fluids, 25, 054102, (2013).

[7] Jalaal, M. and Mehravaran, K., "Fragmentation of falling liquid droplets in bag breakup mode", Int. J. Multiphase Flow, 47, 115, (2012).

[8] Khosla, S., Smith, C.E. and Throckmorton, R.P., "Detailed understanding of drop atomization by gas crossflow using the volume of fluid method", ILASS Americas, 19th, (2006).

[9] Khare, P., Ma, D., Chen, X. and Yang, V., "Phenomenology of secondary breakup of Newtonian liquid droplets", AIAA J., 50, 171, (2013).

[10] Xiao, F., "Large eddy simulation of liquid jet primary breakup", Ph.D. thesis, Loughborough University, (2012).

[11] OpenCFD Ltd., "OpenFOAM 2.1.1 Userguide", OpenCFD Ltd., (2013).

[12] Harvie, D., Davidson, M. and Rudman, M. "An analysis of parasitic current generation in volume of fluid simulations", Appl. Math. Model., 30, 1056, (2006).

[13] Cook, J., Armstrong, L., Luo, K. and Gu, S., "Adaptive mesh refinement of gas–liquid flow on an inclined plane", Comput. Chem. Eng., 60, 297, (2014).

[14] Liovic, P. and Lakehal, D., "Subgrid-scale modeling of surface tension within interface tracking-based large eddy and interface simulation of 3D interfacial flows", Comput. Fluids, 63, 27, (2012).

[15] Hoang, D., Steijn, V., Portela, L. and Kreutzer, M., "Benchmark numerical simulations of segmented two-phase flows in microchannels using the Volume of Fluid method", Comput. Fluids, 86, 28, (2013).

[16] Deshpande, S., Anumolu, L. and Trujillo, M., "Evaluating the performance of the two-phase flow solver InterFoam", Comput. Sci. Disc., 5, 014016-1, (2012).

[17] Brackbill, J., Kothe, D.B. and Zemach, C., "A continuum method for modeling surface tension", J. Comput. Phys., 100, 335, (1992).

[18] Lafaurie, B., Nardone, C., Scardovelli, R. and Zaleski, S., "Modelling merging

and fragmentation in multiphase flows with SURFER", J. Comput. Phys., 113, 134, (1994).

[19] Villier, E., Gosman, A. and Weller, H., "Large eddy simulation of primary diesel spray atomization", SAE 2004-01-0100, (2004).

[20] Jeon, S., Kim, S. and Park, G., "Numerical study of condensing bubble in subcooled boiling flow using volume of fluid model", Chem. Eng. Sci., 66, 5899, (2011).

[21] Höhne, T. and Vallée, C., "Experiments and numerical simulations of horizontal two-phase flow regimes using an interfacial area density model", J. Comput. Multiphase Flows, 2(3), 131, (2010).

[22] Sun, Y. and Beckermann, C., "Sharp interface tracking the phase-field equation", J. Comp. Phys., 220, 626, (2007).

[23] Flock, A., Guildenbecher, D., Chen, J. and Sojka, P., "Experimental statistics of droplet trajectory and air flow during aerodynamic fragmentation of liquid drops", Int. J. Multiphase Flow, 47, 37, (2012).

[24] Chou, W. and Faeth, G., "Temporal properties of secondary drop breakup in the bag breakup regime", Int. J. Multiphase Flow, 24, 889, (1998).

[25] Gao, J., Guildenbecher, R., Reu, P., Kulkarni, V., Sojka, P. and Chen, J., "Quantitative, three-dimensional diagnostics of multiphase drop fragmentation via digital in-line holography", Opt. Lett., 38, 1893, (2013).

[26] Wert, K.L., "A rationally-based correlation of mean fragment size for drop secondary breakup", Int. J. Multiphase Flow, 21, 1063, (1995).

[27] Li, Y. and Lin, M., "Regular and irregular wave impacts on floating body", Ocean Eng., 42, 93, (2012).